# PCCP

Check for updates

# Using a chitosan nanolayer as an efficient pH buffer to protect pH-sensitive supramolecular assemblies

D. V. Andreeva, [a] A. Kollath,[b] N. Brezhneva,[cd] D. V. Sviridov,[c] B. J. Cafferty,[e] H. Möhwald[d] and E. V. Skorb ★[df]

It is attractive to control the properties of macro objects and films by employing simple nanolayer composites, as in the case of nanoarchitectured Layer-by-Layer (LbL) coating. In this paper, we use chitosan as a surface-based pH buffer to protect adsorbed supramolecular fibres from pH-mediated disassembly. Protons are generated on a titania surface under illumination at 405 nm leading to an appreciable pH change on the surface. We find that supramolecular polymers that are highly sensitive to pH change will not disassemble after irradiation if a nanolayer of chitosan is present. We propose that chitosan can be used as an efficient pH-responsive protective layer for pH sensitive soft materials.

## Introduction

Recently[1–3] the pH buffering activity of Layer-by-layer (LbL) assemblies of weak and strong polyelectrolytes was shown to protect metal surfaces. Local pH changes cause corrosion of metal surfaces, but binding of protons to the weak polyelectrolytes was found to inhibit the corrosion events. Thus, a nanolayer with buffering ability, resulting from the chemistry of the LbL architecture, was shown to be critical for protecting a metal surface from corrosion.

A logical continuation of that work was to use local pH changes during irradiation of semiconductor surfaces.[4–8] For example, local pH changes are generated by irradiation of $TiO_2$ surfaces. Light-pH coupling in $TiO_2$/pH sensitive LbL assemblies was shown to be efficient for high-amplitude non-destructive manipulation of soft matter deposited on the semiconductor surface.[4,5] The composite systems were promising for dynamic regulation of adsorption/desorption of proteins,[6] bacteria,[9] and preosteoblast.[5] Thus, dynamic sensors, antifouling coatings and dynamic protein separation and cleaning systems were proposed.

However, the question of proton dynamics within polyelectrolyte-based LbL assemblies remains open. It is unclear if protons are buffered effectively and if pH-sensitive soft matter can be protected against acidification of the local medium.

Here, we examine the ability of a chitosan nanolayer absorbed to a $TiO_2$ surface to stabilize surface-bound supramolecular assemblies against environmental pH change (Fig. 1).
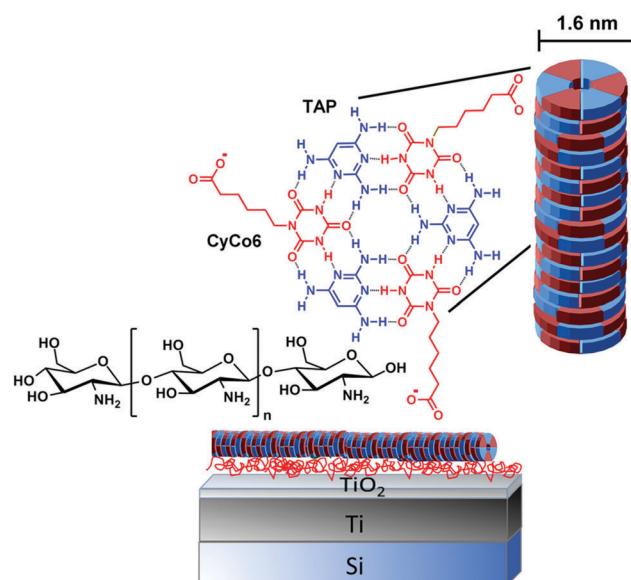


**Fig. 1** Light sensitive $TiO_2$ layer on Si/Ti (negatively charged), positively charged layer of chitosan and negatively charged rosette-based supramolecular polymers of coassembled triaminopyrimidine (TAP) and cyanuric acid modified with hexanoic acid (CyCo6).

[a] *Center for Soft and Living Matter, Institute of basic science, Ulsan National Institute of Science and Technology, 44919 Ulsan, Republic of Korea*

[b] *Physical Chemistry II, University of Bayreuth, Universitätsstraße 30, 95440 Bayreuth, Germany*

[c] *Belarusian State University, 4 Nezavisimosti ave., 220030 Minsk, Belarus*

[d] *Max Planck Institute of Colloids and Interfaces, Am Mühlenberg 1, 14424 Potsdam, Germany. E-mail: skorb@pikg.mpg.de*

[e] *Department of Chemistry and Chemical Biology, Harvard University, 02138 Cambridge, MA, USA*

[f] *Laboratory of Solution Chemistry of Advanced Materials and Technologies (SCAMT) ITMO University St. Petersburg, 197101, Russian Federation*

This journal is © the Owner Societies 2017

*Phys. Chem. Chem. Phys.,* 2017, **19**, 23843–23848 | 23843

Specifically, we investigate the stability of supramolecular polymers formed by triaminopyrimidine (TAP) and cyanuric acid modified with a hexanoic acid side chain (CyCo6), supramolecular polymers that are known to be extremely sensitive to pH change.[10–12]

## Results and discussion

First, we formed a photoactive titania surface suitable for deposition of soft-matter. It is known that the ultraviolet irradiation of photoactive titania generates electron/hole pairs that may induce a photoreaction.[13] The titania is hydrophilic[14] and has a layer of adsorbed water.[15] Reactions with surface adsorbed water molecules can result in a possible pH change on the surface.[16] In the scope of photocatalytic reactions one can assume the possible formation of $H^+$ and $OH^-$ due to oxidation (ox) and reduction (red) reactions involving photogenerated charge carriers on the semiconductor surface. That is, water splitting on a semiconductor can cause the formation of $H^+$ and/or $OH^-$. We recently studied, in detail, the process of water splitting on a titania surface[17] focusing on $H^+$ and $OH^-$ (not $H_2$ and $O_2$ as usual (note, that there is no obvious gas bubbling in our system)) and we observed that this process leads to a pronounced local surface acidification of the irradiated surface and subsequent pH change. The overall pH does not change, although, a pH gradient on the surface may exist.[17] Thus the inorganic surface and its nanostructuring may be involved in the reaction through process location (Fig. 2).

The water oxidation reaction on $TiO_2$ is initiated by a nucleophilic attack of a $H_2O$ molecule on the photogenerated hole at the O site bridging two Ti atoms, and as a result $TiO\cdot HO–Ti$ and later TiOOH and TiOOTi are formed.[18] During these oxygen photoevolution reactions protons are released. At the same time, the photogenerated electrons reduce the surface $Ti^{(4+)}$ enabling adsorption of $H_2O$, and then $O_2$ attacks it immediately to form superperoxo TiOO.[19] As a result a hydroxide ion $OH^-$ is released. Then it is reduced to peroxo Ti(OO) which evolves to
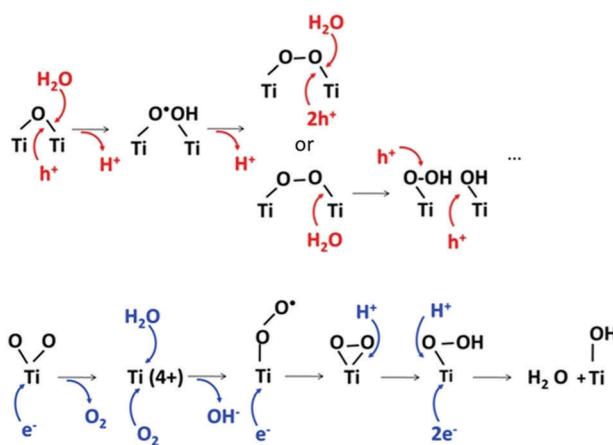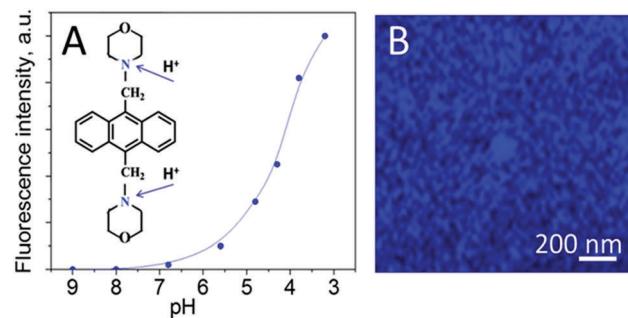


**Fig. 3** (A) Calibration of fluorescent pH indicator, 4,4′-(anthracene-9,10-diyldimethanediyl)dimorpholine, that exhibits a p$K_a \sim 5.1$, and initial chemical formula showing the protonation sites; (B) confocal fluorescent images of the $TiO_2$ surface immediately after irradiation.

hydroperoxo TiOOH upon protonation. At the end, the surface is covered by hydroxyl groups.

This approach can also generate a high concentration of reactive oxygen species and free radicals that may cause degradation of soft matter deposited on the surface of the semiconductor.[10] In order to avoid degradation events, we produced a nanometer thick layer of $TiO_2$ via partial oxidation of a deposited layer of titania on silicon wafers. Morphological properties of the surface after sonochemical treatment were characterized in details in our previous work.[20] It is important here that the ultrasonically generated nanolayer of $TiO_2$ shows mild photoactivity under 405 nm illumination; which produces $H^+$ on the surface. A pH indicator shows an increase in fluorescence, seen in Fig. 3, on the surface after irradiation, corresponding to a pH that is less than 5 on irradiated surface.

We were interested in knowing how many photons are needed to release enough protons from the surface to locally change the pH from 7 to 5. If, for example, a 1 cm² surface of $TiO_2$ is irradiated in order to achieve a pH = 5 (assuming $[H^+] = 10^{-5}$ M or $6 \times 10^{18}$ L$^{-1}$ and a coating with a thickness of 50 nm, that is, $V = 5 \times 10^{-10}$ L), then the concentration of protons in the system is $[H^+] = 3 \times 10^9$ protons cm$^{-2}$, which is about 0.003% of the lattice sites of a typical solid ($10^{15}$ lattice sites cm$^{-2}$). This means that only 0.003% of the surface atoms have to be charged to achieve pH = 5, if no losses exist. Even if we consider a low radiation intensity of 1 mW cm$^{-2}$ = $10^{16}$ photons cm$^{-2}$ s$^{-1}$ for a quantum yield proton/photon conversion of 0.01% the photons from 1 ms irradiation would create enough protons on the $TiO_2$ surface to achieve LbL activation on the surface of $TiO_2$.

The polarization curve recorded under the chopped illumination with 405 nm laser source (shown in Fig. 4) demonstrates that the $TiO_2$ film has a pronounced photoactivity under the illumination, with a photocurrent onset potential of −0.6 V (vs. Ag/AgCl electrode). The observed photosensitivity in the visible range could be attributed to the optical transitions involving electronic states in the forbidden zone which result from highly defective structure inherent in titania generated via intense ultrasonic treatment.[20]

In addition to obtaining a classical I–V curve under chopped illumination we used conductive atomic force microscopy (C-AFM) to perform a local I–V study of the $TiO_2$ surface under



**Fig. 2** Possible reorientation of titania groups and water under irradiation and reactions with photogenerated photohole (h⁺) and photoelectron (e⁻).

23844 | *Phys. Chem. Chem. Phys.*, 2017, **19**, 23843–23848

This journal is © the Owner Societies 2017
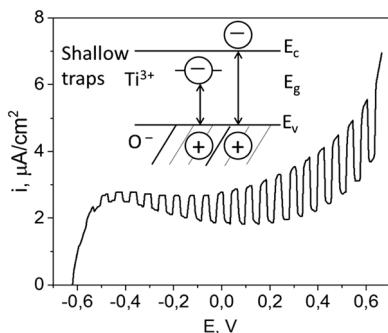
Fig. 4 Photochemical behavior of TiO₂. I–V curve of blank TiO₂ with chopped illumination. Inside schematic shows zone diagram of TiO₂ and suggests possible trapping in forbidden zone that may explain photo-activity during irradiation at 405 nm.
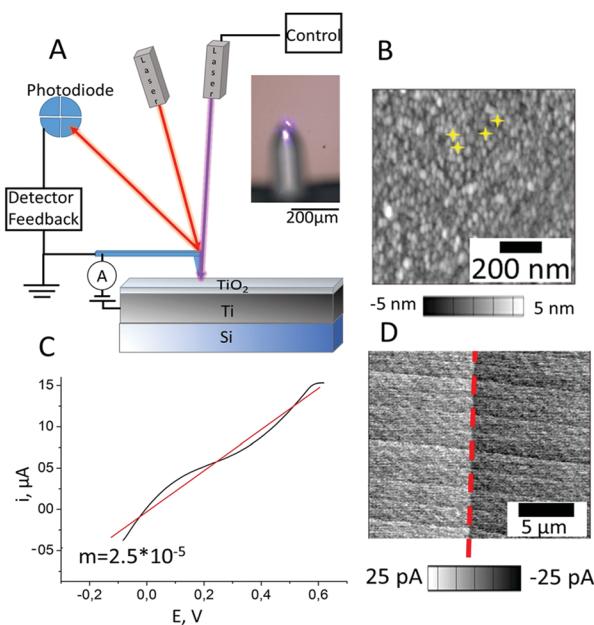


Fig. 5 (A) Atomic force microscopy (AFM) set up for a study of light stimulated processes and changes of multilayer morphology on a semi-conductor surface equipped with an additional UV-laser (inset shows the optical image of an AFM cantilever irradiated with a laser at a certain position of the light spot). (B–D) Conductive AFM (C-AFM) study of TiO₂ layer (B) AFM image showing in yellow certain spots that were used for I–V curve images. (C) Average current vs. voltage (I–V) curve from (B), (D) C-AFM map shows the edge between irradiated and not irradiated part of TiO₂ (clear edge is seen).

illumination. Fig. 5A shows the experimental set-up, there (i) we can use one extra 405 nm laser and focus it in the position of measurement, and (ii) with the use of a special metal (TiIr) tip we can study I–V in specific locations along the surface (examples are shown in yellow in Fig. 5B) and generate a current map. The C-AFM measurements were performed under ambient conditions with very sensitive current detection (from 1 pA). The C-AFM tip was used as a movable electrode to measure the I–V curves on the TiO₂. Fig. 5B shows an average I–V curve that, assuming a linear fit, was used to calculate a TiO₂ resistance of ca. $2.5 \times 10^{-5}$ $\Omega^{-1}$.

In the following we will discuss how the photoactivity of the TiO₂ surface and a series of photocatalytic reactions yields a local change in pH,[8] and triggers conformational changes of pH sensitive soft matter. Previously,[4] we demonstrated that the photons from 10 ms of light irradiation would create enough protons on the TiO₂ surface to achieve conformational changes of polyelectrolytes and LbL assemblies on the surface of TiO₂. It is a high priority of ours to understand how photo-initiated processes on TiO₂ lead to transformation of light into an appreciable pH change, including localization of the effect.

A chitosan layer with a thickness of approximately 2 nm was deposited on titania. Angle-dependent X-ray photoelectron spectroscopy (XPS) measurements (Fig. 6) were used to calculate the layer thickness (d) by measuring the positions of titanium (Ti) atoms in the bottom layer of the surface. Such a method is commonly used to calculate the thickness of self-assembled monolayer (SAM) using the position of the surface-bound sulfur atom.[21]

For these measurements, the free electron mean path exponentially decays with distance. We fixed the position of the analyzer with the lens axis 50° away from the incident beam. The take-off angle (θ) was defined as the angle between the substrate surface and the axis of the analyzer. The incident angle (γ) was defined as the angle between beam incidence and the substrate surface. We rotated the sample holder to collect the Ti2p with θ = 90° (normal emission, γ = 40°) and θ = 40° (normal emission, γ = 90°). To normalize the footprint of incident light between two different angles, the effective intensity (I₀) is given by

$$I_\theta = I\cos(90° - \gamma) \tag{1}$$

where I is the integrated intensity of the peak. The relationship between I₀ and d can be expressed as follow:

$$I_\theta = I\mathrm{e}^{-d/\lambda\sin\theta} \tag{2}$$
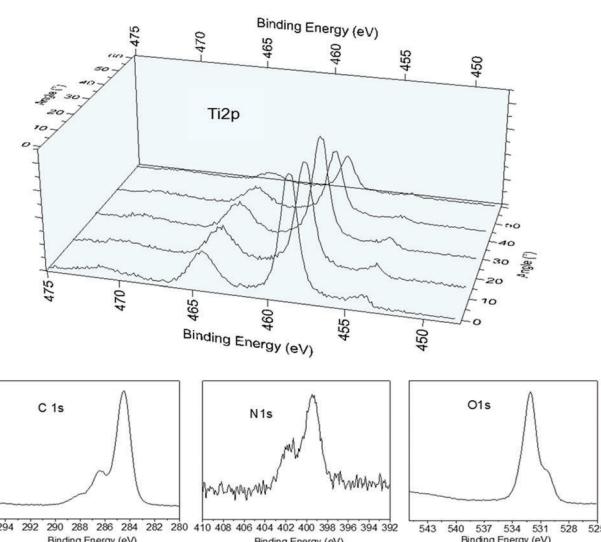


Fig. 6 Angle-dependent high resolution XPS spectrum of Ti 2P for the calculation of chitosan layer thickness and high resolution spectra of C 1s, N 1s and O 1s, proving the chitosan layer is on the surface.

This journal is © the Owner Societies 2017

Phys. Chem. Chem. Phys., 2017, 19, 23843–23848 | 23845

Thus, $I_\theta$ ratio at 90° and 40° take-off angles can be expressed as follows:

$$\frac{I_\theta(d, 90°)}{I_\theta(d, 90°)} = \frac{e^{-d/\lambda \sin 90}}{e^{-d/\lambda \sin 40}} \quad (3)$$

where $\lambda$ is the inelastic mean free path and in our case defined as 30.5 Å. The overlayer thickness $d$ was calculated using eqn (4):

$$d = \frac{\lambda \sin 90° \sin 40° \left[ \ln\left(\frac{I_{90°}}{I_{40°}}\right) \right]}{\sin 90° - \sin 40°} \quad (4)$$

The values of intensity $I$ were fitted by the photoemission profiles with Voigt functions (Lorentzian (30%) and Gaussian (70%)) with Shirley plus linear background corrections.

We also examined the chitosan layer using AFM with simultaneous irradiation of the surface with 405 nm laser before (Fig. 7A and C), during (Fig. 7B and D) and after irradiation (Fig. 8).

The AFM images (Fig. 4A–D) confirm that the surface of chitosan increases in net positive charge under irradiation. For comparison, the effect of smoothing of the chitosan layer by decreasing the solution pH was observed previously by Lee et al.[20] and was explained to result from a change of surface



Fig. 7 (A and B) Phase and (C and D) profile AFM scans of the titania surface at the same position (A and C) before and (B and D) 5 min after illumination with a 2 mW, 405 nm laser. (E) Schematic of proton release from a TiO$_2$ surface during irradiation due to photochemical reactions and chitosan layer protonation. (F) Confocal fluorescence image of the pH indicator, 4,4′-(anthracene-9,10-diyldimethanediyl)dimorpholine, during irradiation of the surface of TiO$_2$ covered with a chitosan layer (TiO$_2$@Chitosan).



Fig. 8 AFM images showing the change of chitosan layer morphology during relaxation of the surface: in 1 min (A), and 10 min (B) after irradiation.

forces due to chitosan protonation. Here, irradiation triggers a local pH change on the semiconductor, and also may cause protonation of chitosan. It is important to note that the layer of chitosan under irradiation remains on the surface and is not detached. An explanation for the stability of the protonated nanolayer on the surface is that together with the rearrangement and structural change of chitosan chains upon protonation, ion diffusion/migration and charge regulation, chitosan forms structured hydrogen-bond networks in humid environments and a practically semicrystalline phase structure. This rigid behavior of chitosan may be a big advantage for using a chitosan nanolayer over other weak polyelectrolyte nanolayers for providing polyelectrolyte assembly stability.

We next employed pH indicators to compare photoinduced pH changes at the surface of pristine TiO$_2$ covered with chitosan (Fig. 7F) vs. bare TiO$_2$ (Fig. 3), to support the buffering activity of the chitosan layer. The pH indicator under irradiation didn't show any fluorescence when surfaces of TiO$_2$ containing a chitosan layer were analyzed, suggesting that the released protons are absorbed by chitosan molecules on the surface, effectively buffering the pH.

After the irradiation is stopped (Fig. 8), slow relaxation of the chitosan film is observed and the polymer layer reaches an equilibrium within app. 10 min. The blurriness of the AFM images can be explained due to simultaneous changes in the surface structure as a result of chitosan relaxation during acquisition.

We next examined the ability of the chitosan nanolayer to protect supramolecular structures from disassembly caused by environmental pH-change (Fig. 9). We chose TAP-CyCo6-based supramolecular polymers due to their ultrasensitive pH response.[10] Supramolecular polymers are formed in water by combining TAP and CyCo6. The monomers self-assemble into hexameric rosette structures, and hydrophobic interactions between rosettes lead to the formation of micron-length supramolecular polymers.[12] The bidirectional pH-response of this supramolecular polymer system results from the presence of an acidic monomer (Cyco6) and a basic monomer (TAP). The pH response is highly sensitive because the p$K_a$s of the monomers are matched at 7, therefore any change in pH from neutrality will cause disassembly of the supramolecular polymers, with complete disassembly at pH below 5.5 and above 8.5.

23846 | *Phys. Chem. Chem. Phys.*, 2017, **19**, 23843–23848

This journal is © the Owner Societies 2017
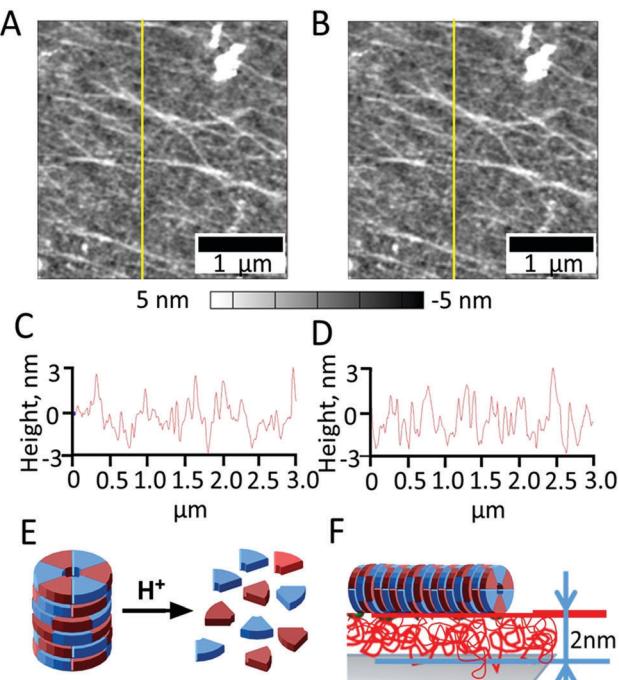
**Fig. 9** AFM images of Layer-by-Layer (LbL) deposited chitosan films on titania followed by TAP/CyCo6 deposition before (A) and after 10 min of irradiation with 9 mW intensity from a 405 nm laser (B), with the corresponding cross sections (C and D). Schematics showing TAP-CyCo6 disassembly resulting from pH-change, and (E) chitosan nanolayer as a proton sponge that affectively protects TAP-CyCo6 supramolecular polymers from disassembly (F).

We next examined if the chitosan nanolayer has enough buffering activity to protect the TAP-CyCo6 supramolecular polymers from pH-mediated disassembly caused by irradiation of the titanium surface (Fig. 6E). The supramolecular polymers were formed in water buffered with sodium phosphate at pH 6.5 and then deposited on the chitosan nanolayer. The AFM image of the surface after TAP-CyCo6 fiber deposition is shown in Fig. 6.

Next, irradiation resulted in photoreactions on the $TiO_2$ surface[4] leading to acidification in irradiated areas. As discussed above, in the absence of chitosan the surface pH would be expected to drop to pH 5, which would disassemble the supramolecular structures. The assemblies were, however, still observed after irradiation, even when irradiation was performed with a laser power of 9 mW for 10 min, demonstrating that chitosan nanolayer has a strong buffering capacity Fig. 6F.

## Conclusions

In order to develop applications for chitosan-based materials, it will be essential to understand the efficiency of chitosan as a buffering material. Here we report that a chitosan nanolayer can be utilized as a proton sponge, thus protecting the integrity of supramolecular assemblies (even those that are highly sensitive to pH variation, such as TAP-CyCo6 assemblies) to surface-mediated pH changes. We provide further evidence here that due to the unique characteristics of chitosan chains, caused in part by

charge pairing with $TiO_2$ and the rigidity of the chains,[22] chitosan may strongly interact with $TiO_2$ and prevent penetration of protons through the chitosan nanolayer, thus protecting supramolecular assemblies associated with the nanolayer surface.

Thus we find that nanolayers of chitosan can be used in the development of surface-based material that are otherwise sensitive to environmental pH change. Particularly, for materials used in double stimuli-responsive devices that are incorporated in living systems, as chitosan exhibits pH protective properties near physiological pH. In spite of many applications of chitosan, there have been few systematic studies conducted with regard to the chitosan nanolayer buffering activity on surfaces.

## Experimental

### Materials

Silicon (Si) wafers (100) were from CrysTech Kristalltechnologie. Absolute ethanol AnalR NORMAPUR from VWR Chemicals was used as received. Low molecular weight chitosan, acquired from Aldrich with a molecular weight between 50 000 and 190 000 Da and a degree of deacetylation (DA) ≥75% was used as received for experiments. Acetic acid was purchased from EMD. Hydrochloric acid (1 M, HCl) and sodium hydroxide (1 M, NaOH) were acquired from Grüssing. Millipore water (Milli-Q Plus 185) was used for preparation of aqueous solutions and sample washing.

### Titania photoactive layer preparation

Si wafers with polished surface were used as substrate for titanium layers of 2 μm thickness deposited by physical vapour deposition using a BA 510 from Fa. Balzers, Liechtenstein. Ti covered Si wafers were fixed in a homemade sample holder for high intensity ultrasound (HIUS) modification. The samples were sonicated for 1 min in ethanol at a sonotrode to surface distance of 5 mm. Cavitation was produced by a UIP1000hd ultrasonic device from Hielscher Ultrasound Technology equipped with a B2-1.8 booster and a BS2d22 sonotrode (head area 3.8 $cm^2$). The operating frequency was 20 kHz with a maximum intensity of 140 W $cm^{-2}$ and an amplitude of 106 μm. The sonication medium was cooled using an ice bath to approximately 333 K.[20]

### Chitosan assembly

Chitosan solution was prepared by dissolving 50 mg of chitosan in 4.95 ml of 1 wt% acetic acid to obtain 1 wt% chitosan solutions (pH ≈ 4). The pH of the chitosan solution was increased to pH 6.5 by addition of aqueous sodium hydroxide solution (0.1 M). Chitosan solution was deposited on the chosen substrates for 10 min by depositing drops of chitosan solution onto the substrates. Afterwards, the substrates were dried using an air pistol. The surface was washed twice.

### Supramolecular assembly

For details on the synthesis of CyCo6 and TAP-CyCo6 supramolecular polymer formation and characterization see ref. 10 Briefly, supramolecular fibers were formed by combining TAP and CyCo6 at 50 mM in an aqueous solution containing 200 mM

This journal is © the Owner Societies 2017

*Phys. Chem. Chem. Phys.,* 2017, **19**, 23843–23848 | **23847**

sodium phosphate (pH 6.5). The solution was then deposited onto a substrate, which had first been prepared with chitosan. The substrate was then washed once with ice-cooled water to remove excess assemblies and phosphate buffer.

Surface characterization was performed using a Cypher S Atomic Force Microscope (AFM) from Asylum Research (Santa Barbara, California) equipped with an OTESPA-R3 Bruker cantilever with a spring constant of 26 N m$^{-1}$ and a frequency of 300 kHz for imaging purposes. For *in situ* irradiation experiments, Asylum Research AC160TS-R3 cantilevers were used with spring constant and frequency corresponding to the OTESPA-R3 Bruker cantilever. The cantilevers were coated with Al in both cases. AFM imaging was carried out in tapping mode. Contact mode was used for conductive AFM using an ORCA cantilever holder (nA, μA) and an Asylum Research ASYELEC-01 cantilever with a spring constant of 2 N m$^{-1}$ and a frequency of 70 kHz. The cantilevers were coated with TiIr with a tip radius of 28+/110 nm. Current–voltage curves were collected from specific surface positions in contact mode driving the sample surface from −4 to +4 V. Current maps of the surface were carried out in contact mode applying no surface bias. A blue laser with a wavelength of 405 nm incorporated into the Cypher S AFM was used as irradiation source. Irradiation power of the laser and irradiation time were varied between 2–9 mW and 1–10 min. The generally chosen laser power of 2 mW corresponds to a laser intensity of approximately 6 μW μm$^{-2}$ given the laser diameter to be approximately 20 μm. An AFM image of the same surface position was taken after every irradiation cycle of 1 min with either the same or increasing laser power. AFM images were analyzed using the Asylum AR14 software. Current–voltage curves were analyzed using Origin Pro.

Photoelectrochemical measurements were performed using a three-electrode quartz cell using titania samples as a working electrode (WE), Pt wire as a counter electrode (CE) and Ag/AgCl (1 M KCl) as a reference electrode (RE) in 0.1 M NaOH solution. The measurements were carried out using a CompactStat potentiostat (Ivium Technologies, the Netherlands). The photodiode with wavelength λ = 410 nm was used as a source of light and kept at a distance 5 cm away from the quartz cell.

### X-ray photoelectron spectroscopy (XPS)

Measurements were performed at the X-ray photoelectron spectroscopy (XPS) measurements were performed with a Scienta ESCA-300 spectrometer. The spectra were taken using a monochromatized aluminum source Al Kα (E = 1487 eV), MX-650 VG Scienta. The base pressure in the analytical chamber was 5 × 10$^{-9}$ mbar. The spectra acquisition was carried out in normal emission geometry with analyzer energy resolution of 0.15 eV. To probe the Ti 2p, C 1s, N 1s and O 1s, their excitation energies were used. The spectra were acquired in normal emission geometry, and the resolution was better than 0.1 eV. The spatial depth distribution of the different elements in the film, XPS spectra were taken at normal emission (90° take-off-angle) and grazing emission (10°) of the photoelectrons and compared. The uncertainty of ±2 Å takes into account the fitting errors and the angular misalignment due to sample mounting.

## Acknowledgements

## Notes and references

1 D. V. Andreeva, D. Fix, H. Möhwald and D. G. Shchukin, *Adv. Mater.*, 2008, **20**, 2789.
2 E. V. Skorb, D. Fix, D. V. Andreeva, H. Möhwald and D. G. Shchukin, *Adv. Funct. Mater.*, 2009, **19**, 2373.
3 D. V. Andreeva, E. V. Skorb and D. G. Shchukin, *ACS Appl. Mater. Interfaces*, 2010, **2**, 1954.
4 S. A. Ulasevich, G. Brezesinski, H. Möhwald, P. Fratzl, F. H. Schacher, S. K. Poznyak, D. V. Andreeva and E. V. Skorb, *Angew. Chem., Int. Ed.*, 2016, **55**, 13001.
5 S. A. Ulasevich, N. Brezhneva, Y. Zhukova, H. Möhwald, P. Fratzl, F. H. Schacher, D. V. Sviridov, D. V. Andreeva and E. V. Skorb, *Macromol. Biosci.*, 2016, **16**, 1422.
6 D. V. Andreeva, I. Melnyk, O. Baidukova and E. V. Skorb, *ChemElectroChem*, 2016, **3**, 1306.
7 Y. Zhukova and E. V. Skorb, *Adv. Healthcare Mater.*, 2017, **6**, 1600914.
8 E. V. Skorb, H. Möhwald and D. V. Andreeva, *Adv. Mater. Interfaces*, 2017, **4**, 1600282.
9 J. Gensel, T. Borke, N. Pazos-Perez, A. Fery, D. V. Andreeva, E. Betthausen, A. H. E. Müller and E. V. Skorb, *Adv. Mater.*, 2012, **24**, 985.
10 B. J. Cafferty, R. R. Avirah, G. B. Schustera and N. V. Hud, *Chem. Sci.*, 2014, **5**, 4681.
11 C. Li, B. J. Cafferty, S. C. Karunakaran, G. B. Schustera and N. V. Hud, *Phys. Chem. Chem. Phys.*, 2016, **18**, 20091.
12 B. J. Cafferty, I. Gállego, M. C. Chen, K. I. Farley, R. Eritja and N. V. Hud, *J. Am. Chem. Soc.*, 2013, **135**, 2447.
13 E. V. Skorb, L. I. Antonouskaya, N. A. Belyasova, D. G. Shchukin, H. Möhwald and D. V. Sviridov, *Appl. Catal., B*, 2008, **84**, 94.
14 E. V. Skorb, E. A. Ustinovich, A. I. Kulak and D. V. Sviridov, *J. Photochem. Photobiol., A*, 2008, **193**, 97.
15 Z. Zhang, K. Yao, Y. Liu, C. Jin, X. Liang, Q. Chen and L.-M. Peng, *Adv. Funct. Mater.*, 2007, **17**, 2478.
16 E. V. Skorb, D. G. Shchukin, H. Möhwald and D. V. Sviridov, *J. Mater. Chem.*, 2009, **19**, 4931.
17 H. Maltanava, S. K. Poznyak, D. V. Andreeva, M. C. Quevedo, A. C. Bastos, J. Tedim, M. G. S. Ferreira and E. V. Skorb, *ACS Appl. Mater. Interfaces*, 2017, DOI: 10.1021/acsami.7b05209.
18 R. Nakamura and Y. Nakato, *J. Am. Chem. Soc.*, 2004, **126**, 1290.
19 R. Nakamura, A. Imanishi, K. Murakoshi and Y. Nakato, *J. Am. Chem. Soc.*, 2003, **125**, 7443.
20 A. Kollath, N. Brezhneva, E. V. Skorb and D. V. Andreeva, *Phys. Chem. Chem. Phys.*, 2017, **19**, 6286.
21 O. Dannenberger, K. Weiss, H. J. Himmel, B. Jager, M. Buck and C. Woll, *Thin Solid Films*, 1997, **307**, 183.
22 D. W. Lee, C. Lim, J. N. Israelachvili and D. S. Hwang, *Langmuir*, 2013, **29**, 14222.